Geological, Geochemical and Microthermometry Investigations of Manganese Prospects, Ophiolite-Hosted of Birjand, East of Iran†

Behnaz Barghi [1], **Ahmad Azargoon Jahromi** [2,*]

[1] Geology Department, University of Birjand, Iran E-mail: barghibehnaz@yahoo.com
[2] Mining and Metallurgical Engineering Department, University of Yazd, Iran E-mail: ahmad.azargoon@gmail.com
[*] Correspondence: ahmad.azargoon@gmail.com
[†] Presented at the title, place, and date.

Abstract: The studied manganese prospects are located in ophiolitic complex of Birjand, east of Iran. The ophiolitic sequence in this region hosts manganese ores occurring as lens associated with radiolarian cherts and as veinlets with shales. The main gangue minerals are calcite, silica and gypsum. The major manganese ore minerals are pyrolusite, braunite, bixbyite, ramsdellite, and romanechite showing replacement, colloidal, and brecciated textures. High concentration values of Si, Fe, Mn, Ba, Zn, Sr, and As in the studied manganese ores can be applied as evidence for sea-floor Mn-rich hydrothermal exhalatives responsible for the formation of the ores. Investigations on fluid inclusions of calcites demonstrated that the ore-forming solutions had salinities within the range of 0.5-4.5 wt% NaCl eq., homogenization temperature range of 100-220°C and density about 0.8-1 g/cm³. The pressure was estimated to be about 50 bars which corresponds with a depth of ~150 meters at the time of formation manganese prospects that fluid inclusions datas approved hydrothermal processes in the studied manganese prospects can be applied as evidence for sea-floor Mn-rich hydrothermal exhalatives responsible for the formation of the ores. The geological and geochemical results also revealed that deposition of the ores occurred on upper parts of the ophiolitic sequence by submarine exhalatives. The hydrothermal activities caused leaching of elements such as Mn, Fe, Si, Ba, As, and Sr from basaltic lavas (spilites) through concurrent faults with deposition, elements entered to sedimentary basin and during the retreat of the sea with the expansion of oxidation conditions are formed the primary manganese minerals were Mn oxides and hydroxides which have gradually been converted to psilomelane and finally pyrolusite, braunite and bixbyite.

Keywords: Radiolarian; chert; Ophiolite; Manganese; Geochemistry; Fluid inclusion; submarine exhalatives

1. Introduction

Hydrothermal deposits are of small size and occur as irregular bodies in the marine environment, proximate to the spreading centers or in subduction-related island arc settings (Heshmatbehzadi and Shahabpour, 2010). The origin of hydrothermal Mn deposits in marine environments is a matter of debate. The ophiolitic sequence in the Birjand area (east of Iran) is comprised mainly of ultramafic rocks and indicates a well-developed mid-oceanic to supra-subduction ophiolite complex of Mid-Cretaceous age (Zarrinkoub et al., 2012). Radiolarian cherts, metacherts and shales outcropped in the ophiolite are intensely fractured or folded. The cherts are found in a variety of colors ranging from light to dark red. That of dark red contain small Mn deposits of lens and greenish white shales contain vein-veinlets types. Although most of the Mn deposits in Birand (Makhunik, Kanif and Sahlabad) are small with changing grade and periodically examined as a potential source for Mn ore,

no detailed study on the mineralization had been performed. The aim of this paper is to discuss the genesis and microthermometry considerations of manganese prospects ophiolite-hosted of Birjand, east of Iran.

Material and Methods

Random and systematic sampling was done along seven cross sections perpendicular to ore trending in order to sample all cherts, shales and ore types. Laboratory investigations include petrographic examinations of 79 thin-polished sections under microscope. To accurately identify the manganese mineral phases, 9 ore samples were analyzed by X-ray diffraction (XRD) method (Phillips Diffractometer, model 1840, CuKα radiation, graphite chromators, voltage 40kV, current 30 mA, scanning speed 2ɵ per minute, scan range (2-70°) in the Geology Department, University of Birjand. Also, 9 ore samples were chemically analyzed by using ICP-OES-MS, and ICP-MS methods in ACME labs, Canada for major, minor and trace elements (see Table 2). Six doubly-polished wafers were prepared for fluid inclusion studies. Microthermometric analyses were carried out by using Linkam-TH-600 stage in Iran Mineral Processing Research Center, Karaj.

Discussion:

1. Geological setting and field description

The Sistan suture zone in the east between Hilmand Block and Lut Block, (Aghanabati, 1998; Ramezani & Tucker., 2003). In an area of 800 km wide and 200 km wide, there are thick accumulations of flysch Accumulated that have ophiolite basement rock dependent on the oceanic crust. Which has accepted the stages of development from the oceanic crust to the continent, is one of the derivations of the Neo- Tethys, which it has names such as flysch and colored melange (Stocklin et al., 1973) and Sistan suture zone (Tirrul et al., 1983). Which includes various deposits Particular manganese prospects in Makhunik, Kanif, and Sahlabad are located about 110 km, 150 km, and 175 km, respectively in southeast of Birjand, South-Khorasan province. They lie on the upper parts of the ophiolitic sequence in the east of Iran (Fig.1). There are igneous units of the sequence are mainly serpentinized peridotite, rodingitic gabbro and spilitized basaltic pillow lavas and sedimentary units are chiefly radiolarian chert and shale and pelagic limestone, which overlie the spilites. The manganese ores occurred as discontinuous patches associated with radiolarian chert and shale .
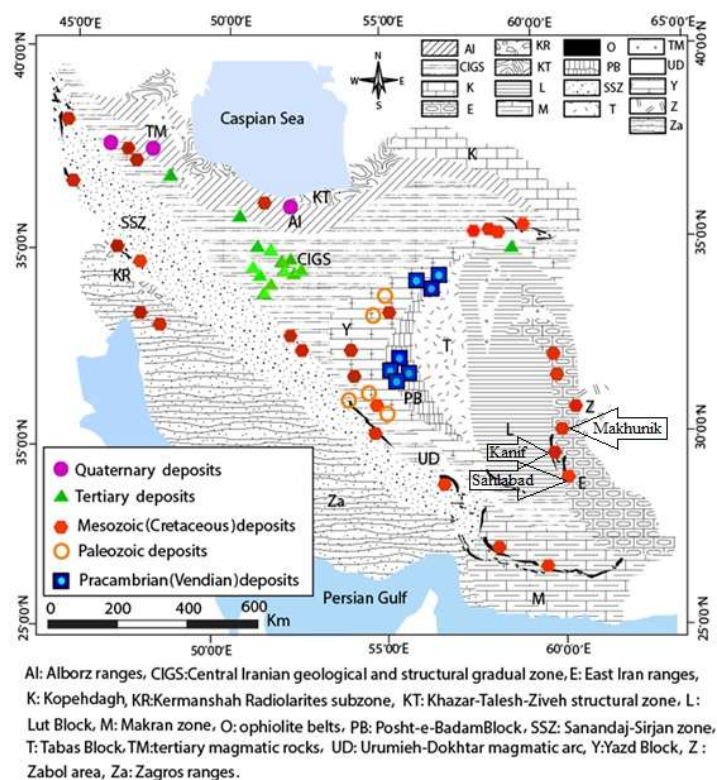
AI: Alborz ranges, CIGS:Central Iranian geological and structural gradual zone, E: East Iran ranges,
K: Kopehdagh, KR:Kermanshah Radiolarites subzone, KT: Khazar-Talesh-Ziveh structural zone, L:
Lut Block, M: Makran zone, O: ophiolite belts, PB: Posht-e-BadamBlock, SSZ: Sanandaj-Sirjan zone,
T: Tabas Block, TM:tertiary magmatic rocks, UD: Urumieh-Dokhtar magmatic arc, Y:Yazd Block, Z :
Zabol area, Za: Zagros ranges.

Figure 1. Geological map showing litho-tectonic domains in Iran and Distribution map of manganese deposits and indices by age (Aghanabati, 1998). The location of the study area is also shown on the map (modified by Barghi, 2017).

2. The main ore mineralogy

Based upon microscopic examinations of thin-polished sections and the XRD analysis results (Table1), the manganese ores consist principally of pyrolusite, braunite, and bixbyite accompanied by lesser amounts of ramsdellite and romanechite. Fe-oxide phases include lesser amounts of hematite and goethite. Hematite occurs as anhedral and bladed aggregates (Fig.2b), while pyrolusite and braunite are massive. Bixbyite occurs as rhombohedral crystals (Fig.2c). Romanechite shows colloidal texture (Fig.2L).

Table 1. Results of X-ray diffraction (XRD) analysis of three types of Mn ores in the studied areas.

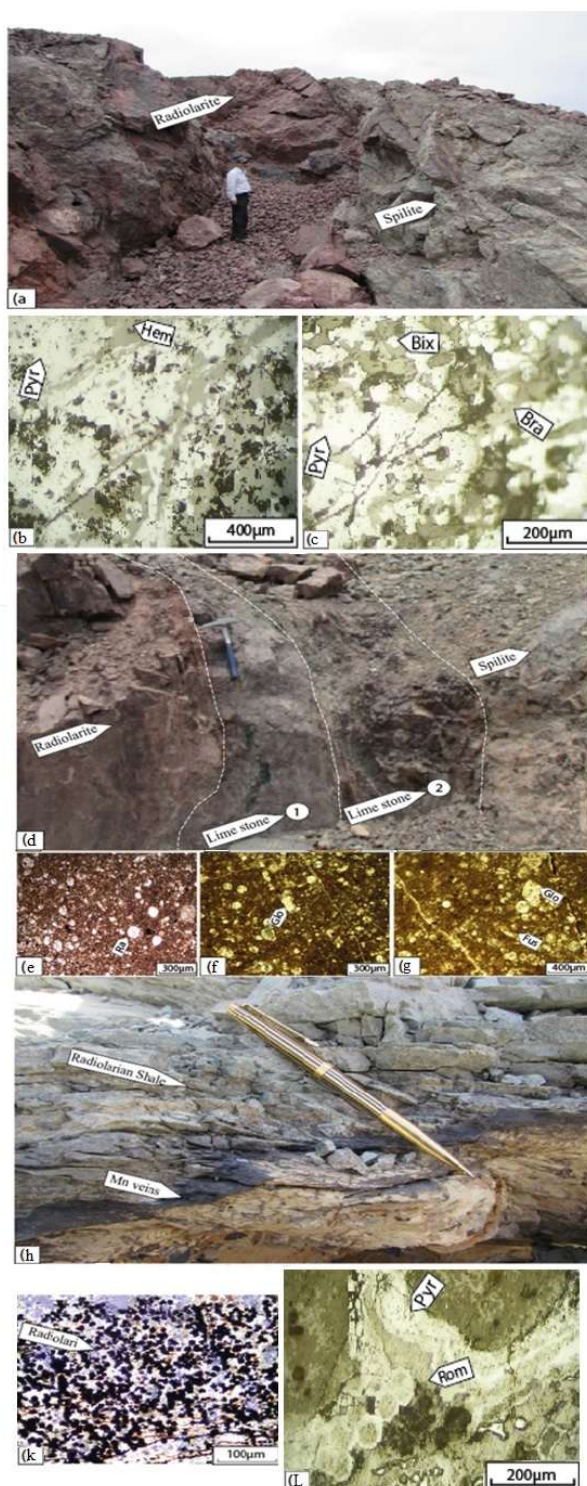| Samples	Major phases	Minor phases	Trace phases
Kanif	Quartz	Pyrolusite, Hematite	-
Makhunik	Quartz	Pyrolusite, Braunite, Bixbyite, Hematite	Calcite-Chabasite-Goethite
Sahlabad	Quartz	Pyrolusite,Psilomelane Hematite	Romanechite, Ramsdellite,Goethite

Figure 2. Field photos of Mn-bearing lenses, veins and Photomicrographs. (a) Lens structure in dark red chert in Makhunik. (b) Hematite and pyrolusite in light red chert (PPL). (c) Pyrolusite, bixbyite, and braunite showing replacement texture in dark red to brown chert (PPL). (d) Lens of Mn ores in red to brown chert in Kanif. (e) Photomicrographs of Radiolarite in Kanif (XPL). (f) Photomicrographs of green limestone with Globotroncana microfossils (XPL). (g) Photomicrographs of brown limestone with Globotroncana microfossils (XPL). (h) Mn-vein in green shale in Sahlabad. (k) Photomicrographs of Radiolarian green shale replaced by Mn (XPL). (L) Pyrolusite and romanechite displaying colloidal texture in green radiolarian shale (PPL).

3. Manganese mineralization

Manganese ores in the three studied prospect areas occurred as lenses and veins/veinlets within the sedimentary hosts (pelagic radiolarian chert and shale), which in turn are affiliated with ophiolitic complex (see Fig.4). The ores in these prospects lack deep root and much lateral extent. Two stages of manganese mineralization were recognized in the studied areas, diagenetic and epigenetic. Based upon field relations, The Mn ores localized within the dark-red to brown radiolarian chert are lenticular (~6.5 m thick and 5-20 m length), and display diagenetic feature. Lens structure in dark red chert in Makhunik (Fig.2 a). Lens of Mn ores in red to brown chert in Kanif (Fig.2 d). Radiolarian red to brown chert containing Mn (Fig.2 e) with green and brown limestone (Fig.2 f, g). The epigenetic Mn ores occurred dominantly as veins/veinlets within the green radiolarian shale in Sahlabad (Fig.2 h). Mineralogically, the Mn ores of diagenetic origin contain mainly pyrolusite, braunite, bixbyite and hematite accompanied by gangue minerals such as calcite, chabasite, goethite and quartz. Of these, braunite is the diagnostic Mn-bearing mineral phase, being stable in all diagenetic stages. The epigenetic ores also have mainly psilomelane, pyrolusite and hematite, which are accompanied by lesser amounts of ramsdellite and romanechite. Goethite and quartz are the principal gangue minerals. The average grades of manganese ores in Makhunik, Kanif and Sahlabad are about 39.85%, 33.92% and 31.60%, respectively (see Table 2).

4. Geochemical investigation

Geochemical data can be used as essential criteria for distinguishing various manganese deposits including hydrothermal, diagenetic, epigenetic and biogenetic-microbial (Polgari et al., 2012). Therefore, some major and minor elements can be used to identify manganese deposits formed under various conditions in geological environments (Crerare et al., 1982). In order to identify the type of manganese mineralization in the studied areas, ratios of Mn/Fe and Si/Al and diagrams such as Mn-Fe-(Co+Cu+Ni)*10, U-Th and Pb-Zn were used in this context (Table2). The high value of Si/Al can be indicative of submarine exhalative activities. In manganese deposits with detrital origin, the concentration of Al is relatively greater than Si, which is due mainly to break down of terrigenous feldspars (Crerar et al., 1982; Bonatti, 1975; Nicholson, 1992a; Roy, 1992). Holtstam and Mansfeld (2001) believe that if manganese ores of hydrothermal origin were mixed with detrital particles, the Si/Al ratio would decrease. This ratio for the studied ores is 5.15 in Makhunik, 35.03 in Kanif, and 6.78 in Sahlabad, all of which are within the range of hydrothermal ore deposits (Fig.3a). The concentration value of U in hydrothermal Mn deposit is a few times greater than that of hydrogenous-type one (Bonatti et al., 1976; Bonatti, 1975; Crerar et al., 1982). The presence of Th in Mn deposits is attributed to detrital materials and is not influenced by geochemical processes in marine environment (Maynard, 2010). Because of the low solubility and short residence time, thorium cannot be dissolved in sea water. Uranium is also enriched by hydrothermal activities (Heshmatbehzadi and Shahabpour, 2010). According to Fig.3b, the U enrichment in the studied samples is due to the hydrothermal activities. Fig.3c the main distinguishing criteria in this diagram are the concentration values of Cu, Co and Ni. In hydrothermal Mn deposits, the total values of elements such as Co, Ni and Cu are <1% (Toth, 1980; Usui and Someya, 1997). Since the total values of these three elements in the studied ore samples are <1%, suggesting hydrothermal origin for all three manganese prospects. Depositional environment of manganese can be determined by using Pb-Zn bivariate plot (Nicholson, 1992b). According to Fig.3d, all the data points of the studied Mn deposits (at Makhunik, Kanif and Sahlabad) plotted in the field of volcano-sedimentary (SEDEX).
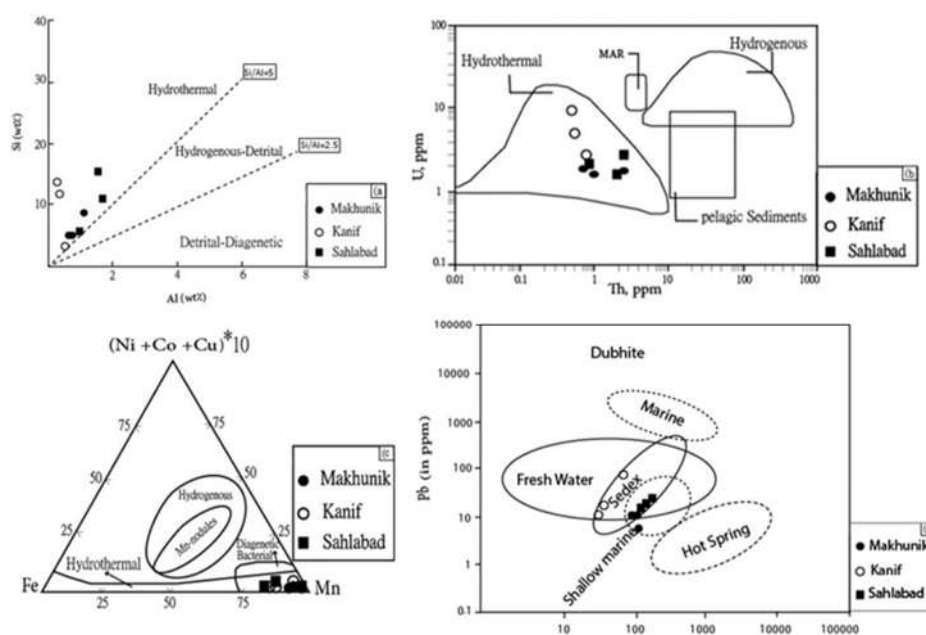
Figure 3. (a) Bivariate plot of Si versus Al (Choi &Hariya, 1992) in which, data points of the ore samples fall within the hydrothermal domain. (b) Ternary plot of Fe-Mn-(Ni+Co+Cu) ×10 (Toth, 1980; Bonatti, 1975) with the plotted data points within the hydrothermal field.(c) Bivariate plot of U versus Th (Bonatti et al., 1976) in which, data points of the studied Mn ores lie within the hydrothermal domain.(d) Bivariate plot of Pb versus Zn (Nicholson, 1992a) in which, data points of the analyzed Mn ores (Makhunik, Kanif, and Sahlabad) lie within the Sedex (sedimentary-volcanic) field.

Table 2. Geochemical results of 9 selected Mn ore samples from the studied areas for major, minor, and trace elements, using ICP-ES-MS and ICP-MS methods.

		Makhunik			Kanif			Sahlabad			
		Sample	number		Sample	number		Sample	number		
element	MDL[*]	M-43	M-44	M-47	63K-	K-64	K-70	S-82	S-86.1	S-86.2	average
Mo	0.5ppm	7.8	9.0	6.2	246.6	161.1	121.8	14.4	9.5	20.2	66.28
Cu	0.5ppm	97.1	112.1	140.2	20.3	35.6	99.6	31.5	183.7	53.0	85.9
Pb	0.5ppm	16.9	11.4	8.6	156.6	75.1	27.0	41.3	76.8	55.2	52.1
Zn	5ppm	241	183	253	75	48	42	116	219	164	149
Ag	0.5ppm	<0.5	<0.5	<0.5	<0.5	<0.5	<0.5	<0.5	<0.5	<0.5	<0.5
Ni	0.5ppm	860.3	402.5	528.9	18.5	14.0	26.2	88.2	203.7	106.8	249.9
Co	1ppm	473	555	464	29	19	16	77	108	98	204.3
Mn	5ppm	39.56%	36.31%	43.67%	28.87%	27.85%	45.04%	35.44%	34.30%	25.06%	35.12%
Fe	0.01%	1.33	1.82	1.07	4.85	4.67	2.40	5.14	5.76	6.28	3.70
As	5ppm	2464	187	898	681	599	316	77	40	130	599.1
U	0.5ppm	2.5	2.4	2.2	7.8	5.0	2.7	2.1	2.7	1.6	3.22
Th	0.5ppm	0.7	2.3	1.0	<0.5	<0.5	0.8	0.8	2.6	1.8	1.42
Sr	5ppm	3779	683	588	3678	1367	1775	3179	1330	3177	2172.8
Cd	0.5ppm	1.6	<0.5	<0.5	<0.5	<0.5	<0.5	1.0	0.9	0.7	1.05
Sb	0.5ppm	225.4	11.6	21.2	2.4	5.2	2.2	3.0	179.2	2.9	50.34
Bi	0.5ppm	<0.5	<0.5	<0.5	<0.5	<0.5	<0.5	<0.5	<0.5	<0.5	<0.5
V	10ppm	264	482	207	146	92	121	29	57	62	162.2
Ca	0.01%	4.23	6.43	5.44	1.36	1.55	3.72	2.04	0.56	1.20	2.94
P	0.01%	0.03	0.03	0.03	0.01	<0.01	0.03	0.04	0.05	0.04	0.032
La	0.5ppm	6.7	9.2	7.2	1.1	0.6	4.6	7.3	12.8	8.9	6.48
Cr	1ppm	62	49	45	9	14	14	18	35	26	30.22
Mg	0.01%	0.53	0.77	0.81	0.26	0.16	0.61	0.49	0.36	0.39	0.48
Ba	5ppm	6273	3094	1312	196	338	32	1170	1363	3176	1883.77

Ti	0.01%	0.054	0.156	0.107	0.006	0.003	0.051	0.045	0.143	0.099	0.073
Al	0.01%	0.99	1.78	0.94	0.29	0.20	0.85	1.33	1.86	1.68	1.10
Na	0.01%	0.68	0.04	024	0.30	0.15	0.36	1.08	0.66	0.58	3.09
K	0.01%	0.22	0.04	0.14	0.10	0.07	0.08	0.42	0.49	0.47	0.22
W	0.5ppm	5.0	3.7	3.2	63.6	65.5	103.6	0.5	<0.5	0.8	30.73
Zr	0.5ppm	12.2	34.5	19.6	1.6	1.1	11.4	8.6	23.2	9.3	13.5
Ce	5ppm	14	20	11	<5	<5	<5	18	32	27	15.7
Sn	0.5ppm	<0.5	0.9	<0.5	<0.5	<0.5	<0.5	0.8	0.7	0.7	0.77
Y	0.5ppm	18.8	11.7	12.7	2.0	1.8	4.5	47.8	32.3	21.0	16.95
Nb	0.5ppm	1.6	4.5	2.3	<0.5	<0.5	0.8	1.6	5.7	4.3	2.97
Ta	0.5ppm	<0.5	<0.5	<0.5	<0.5	<0.5	<0.5	<0.5	<0.5	<0.5	<0.5
Be	5ppm	<5	<5	<5	<5	<5	<5	<5	<5	<5	<5
Sc	1ppm	2	7	3	<1	<1	3	3	8	5	4.42
Li	0.5ppm	4.7	1.9	10.0	15.7	8.7	7.9	26.7	13.5	21.7	12.31
S	0.05%	0.12	0.12	0.09	0.09	0.07	0.10	<0.05	0.07	<0.05	0.094
Rb	0.5ppm	5.7	3.3	5.7	1.4	2.0	1.7	10.8	17.7	16.7	7.22
Hf	0.5ppm	<0.5	0.9	0.6	<0.5	<0.5	<0.5	<0.5	0.6	<0.5	0.7
Se	5ppm	<5	<5	<5	<5	<5	<5	<5	<5	<5	<5
SiO_2	0.01%	10.54	19.97	10.58	23.15	27.31	7.32	12.3	25.18	35.13	19.05
Si	0.01%	4.92	9.32	4.94	10.81	12.75	3.41	5.74	11.76	16.41	8.89
Si/Al		4.97	5.24	5.25	37.29	63.79	4.022	4.32	6.32	9.7	15.65
Mn/Fe		29.75	19.95	40.81	5.95	5.96	18.7	6.89	5.95	3.99	15.32

5. Microthermometric investigation

Fluid inclusion studies can provide better perception of physico-chemical (temperature, pressure, and salinity) and evolution of the ore-forming hydrothermal fluids (Roedder, 1979, 1984; Spooner, 1981). Six doubly-polished sections were prepared to study fluid inclusions in calcite and quartz crystals associated with Mn minerals. Of six, 2 sections from the Makhunik had inclusions in quartz crystals <4 μm and 2 sections from the Sahlabad contained inclusions in calcite crystals <4 μm which were recognized to be unsuitable for microthermometric analysis. Only two sections from the Kanif contained inclusions within the range of 1-20 μm which were chosen for microthermometric analysis. Twenty six fluid inclusions in calcite crystals within these two sections were analyzed for homogenization temperature (TH) and salinity, and the results are listed in Table 3. Petrographic examinations showed that temporally three types of inclusions are present, (1) primary, (2) pseudo-secondary, and (3) secondary. The shapes of inclusions vary from rounded, sub-rounded, stretched, ellipsoidal (Fig.4a, b) elongate, stretched ellipsoidal, Rectangular and rod shapes (Fig.4c, d) Rhombic shape and on the basis of phase content, the majority of them are liquid-rich 2-phase.
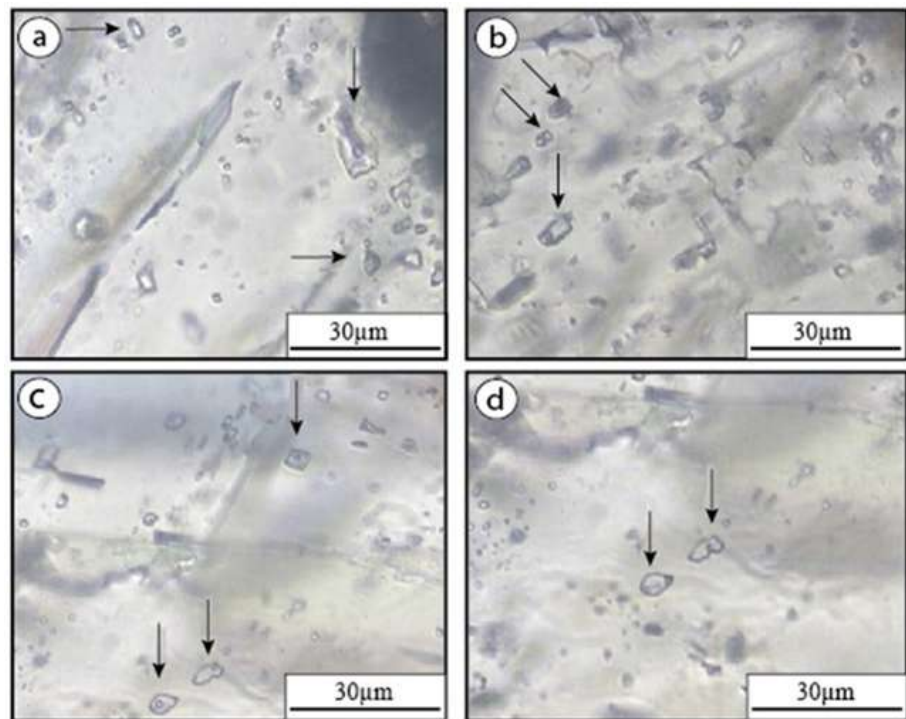
Figure 4. Photomicrographs of various shapes of fluid inclusions within calcite crystals of the Mn ores at Kanif. (a, b) elongate, stretched ellipsoidal, Rectangular and rod shapes. (c, d) Rhombic shape.

Table 3. Microthermometric data obtained from fluid inclusions within calcite crystals in the Mn ores at Kanif.

Sample	n	Size (µm)	Type	Tm (ice) °C	wt% NaCl	TH(L-V) °C
014-Br-56	1	8	L+V	-0.5	0.6	150
	2	8	L+V	-0.5	0.6	148
	3	7	L+V	-1.2	1.94	146
	4	10	L+V	-2.2	3.73	143
	5	10	L+V	-2.1	3.56	140
	6	8	L+V	-2.4	4.07	150
	7	7	L+V	-2.1	3.56	151
	8	22	L+V	-2.1	3.56	165
	9	1	L+V	-2.1	3.56	168
	10	8	L+V	-2.3	3.9	160
	11	1	L+V	-2.2	3.73	155
	12	6	L+V	-2.1	3.56	145
	13	7	L+V	-1.5	2.5	152
	14	7	L+V	-1.5	2.5	148
	15	7	L+V	-2.4	4.07	150
	16	8	L+V	-1.2	1.94	160
	17	5	L+V	-1.2	1.94	150
	18	7	L+V	-1.8	3.03	144
	19	7	L+V	-0.9	1.38	138

	20	7	L+V	-0.9	1.38	140
	21	8	L+V	-1.5	2.5	140
	22	12	L+V	-1.8	3.03	170
	23	8	L+V	-1.2	1.94	130
	24	9	L+V	-1.2	1.94	128
	25	10	L+V	-1.2	1.94	130
	26	8	L+V	-1.2	1.94	135
	27	18	L+V	-1.2	1.94	128
	28	12	L+V	-1.2	1.94	135
	29	10	L+V	-1.2	1.94	135
	30	5	L+V	-2	3.39	267
	31	6	L+V	-1.8	3.03	169
	32	10	L+V	-2.5	4.24	215
	33	10	L+V	-2	3.39	282
	34	8	L+V	-1	1.57	200
	35	8	L+V	-1	1.57	204
	36	5	L+V	-1.5	2.5	218
	37	8	L+V	-1.8	3.03	120
	38	15	L+V	-2.5	4.24	117
	39	10	L+V	-2.5	4.24	115
	40	10	L+V	-1	1.57	115
	41	6	L+V	-1	1.57	125
	42	6	L+V	-1.5	2.5	106
	43	10	L+V	-1.5	2.5	115
	44	10	L+V	nv	.....	114
014-Br-57	45	8	L+V	nv	.....	125
	46	5	L+V	nv	.....	129
	47	6	L+V	nv	.....	125
	48	7	L+V	nv	.....	115
	49	5	L+V	nv	.....	115
	50	5	L+V	nv	.....	125
	51	9	L+V	nv	.....	125
	52	7	L+V	nv	.....	130
	53	8	L+V	nv	.....	130
	54	5	L+V	nv	.....	100
	55	9	L+V	-1.6	2.68	125
	56	5	L+V	-0.6	0.80	130
	57	5	L+V	-1.5	2.5	100
	58	6	L+V	-1	1.57	155
	59	5	L+V	-1.5	2.5	125
	60	5	L+V	-1.7	2.86	125

61	5	L+V	-1.7	2.86	120
62	8	L+V	-1.4	2.31	135
63	5	L+V	-1.4	2.31	117
64	5	L+V	-1.5	2.5	185
65	5	L+V	-1.5	2.5	115
66	5	L+V	-1.6	2.68	145
67	5	L+V	-1.5	2.5	135
68	6	L+V	-1.5	2.5	118
69	8	L+V	-1.5	2.5	155
70	5	L+V	-1.7	2.86	160
71	5	L+V	-1.4	2.31	125
72	8	L+V	-1.3	2.13	196
73	8	L+V	-0.7	0.99	180
74	8	L+V	-0.7	0.99	178
75	8	L+V	-0.7	0.99	150
76	7	L+V	-0.9	1.38	150
77	7	L+V	-0.7	0.99	206
78	5	L+V	-1	1.57	195
79	12	L+V	-1.7	2.86	190
80	15	L+V	-1.3	2.13	190
81	10	L+V	-1.6	2.68	185
82	7	L+V	-1.7	2.86	180
83	12	L+V	-1.7	2.86	190
84	10	L+V	-1.7	2.86	185
85	12	L+V	-1.3	2.13	189
86	9	L+V	-1.3	2.13	185
87	8	L+V	-0.7	0.99	175
88	12	L+V	-0.7	0.99	180

5.1. Microthermometric analysis

The microthermometric analysis was performed principally on inclusions which were relatively large (>5 μm) and liquid-rich 2-phase. They exhibit a limited range of variation in salinity (0.5-4.5 wt% NaCl eq.) (Fig.5a), and were homogenized into liquid state. Their homogenization temperatures (TH) vary from 100°C to 220°C (Fig.5b). The bivariate plot of TH versus salinity (Fig.6a) demonstrated that the inclusions trapped under-saturated fluids within the temperature range of 100-220ºC under pressure <50 bars. The obtained densities for these fluids vary from 0.8 g/cm³ to 1 g/cm³ (Fig.6b).
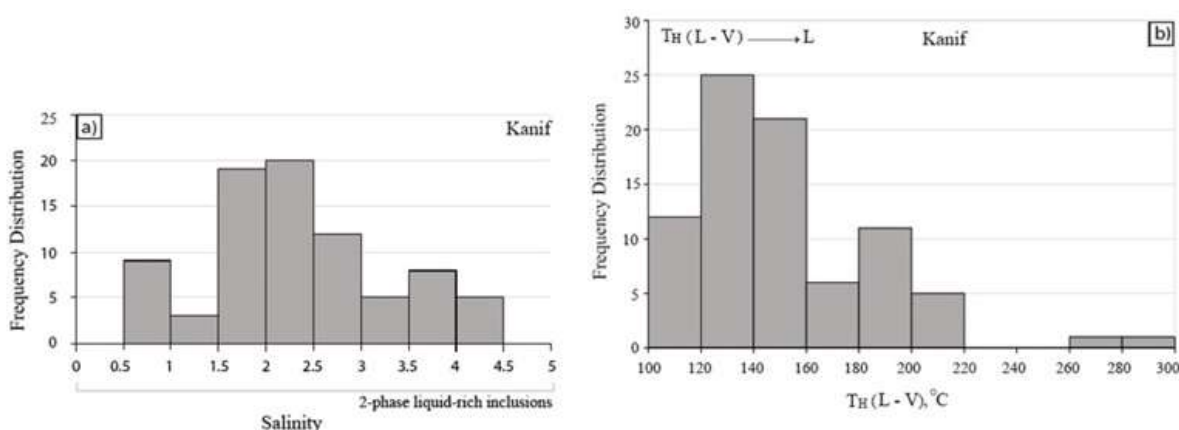
Figure 5. (a) Histogram showing the measured solubility of the liquid-rich 2-phase inclusions in calcite crystal at Kanif.(b) Histogram showing the measured homogenization temperature (TH) of the liquid-rich 2-phase inclusions in calcite crystal at Kanif.
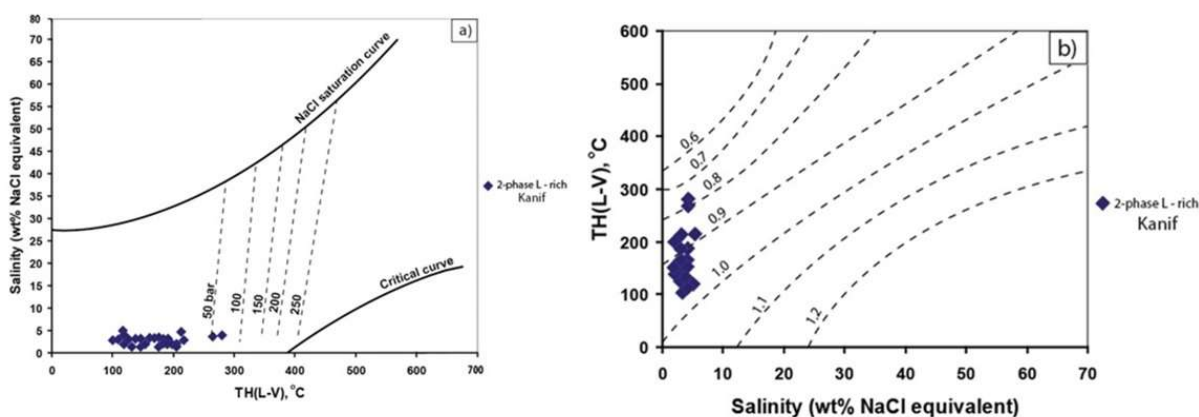

Figure 6. (a) Bivariate plot of $TH_{(L-V)}$ versus salinity. Shown on this figure are also the halite saturation curve, critical curve (Ahmad and Rose, 1980), and the dashed lines representing the homogenization pressures of the fluid inclusions at the indicated temperature and salinity (Roedder, 1984). (b) plot of $TH_{(L-V)}$ versus salinity (expressed as wt% NaCl eq.) showing densities (in g/cm^3) of the studied liquid-rich 2-phase fluid inclusions (Wilkinson, 2001). Contours regressed from data generated by the equation-of-state of Zhang and Frantz (1987).

6. Genesis of the Mn ores

Based upon data obtained from field relations, petrographic examinations, and geochemical studies, the studied manganese ores are genetically related to sea-floor hydrothermal exhalative systems. Hydrothermal solutions derived from the interaction of heated seawater with volcanic rocks at the oceanic floor; following the deep sea convection, leach out Mn and other elements such as Fe and Si in volcanic rocks (Roy, 1992). These metal-bearing solutions ascend through fracture zones and precipitate rapidly most of the metals during the mixing of the hot, acidic and reducing metallic-bearing solutions with cold, alkaline and oxygenated seawaters at the sea floor. Manganese segregation from seawater occurs by precipitation of primary Mn-oxides (hollandite, todorokite, psilomelane, romanechite) accompanying silica gel. An increase in pressure and temperature results in further gravitative fractionation of Mn oxides and Mn hydroxides from silica and consequently the formation of minor braunite in the ore. The most common geochemical feature of hydrothermal Mn-bearing deposits is fractionation of Fe from Mn due to initial precipitation of Fe-bearing minerals at higher temperatures and lower Eh conditions, while manganese is soluble in wide Eh-pH ranges and low temperatures and hence, can be transported over longer distances (Mücke et al., 1999) and is precipitated at higher Eh in the distal sediments within radiolarian cherts and shales, following cooling and/or mixing (Jach and Dudek, 2005).

1

7. Conclusions

2

Based field studies, and distribution of petrographic, mineralogical, microtextural, geochemical manganese prospects in the studied areas (Makhunik, Kanif, and Sahlabad) lie on the upper parts of the ophiolitic sequence of mid to late Cretaceous age. Manganese ores in the studied areas occurred as lenses and veins/veinlets, within radiolarian cherts and shales. manganese ores are pyrolusite, braunite, bixbyite, romanechite and ramsdellite along with iron oxide (hematite), showing chiefly replacement, colloidal and brecciated textures.

3
4
5
6
7
8
9

Geochemical investigations based upon major and trace elements indicated that the high ratios of Mn/Fe and Si/Al, bivariate plots of Pb-Zn and U-Th, and the low concentration values of Cu, Ni and Zn, and the high values of Si, Fe, Mn, Zn, Sr and As strongly testify (sedimentary-volcanic) environment for the Mn ores in the studied areas. According to microthermometric data obtained from fluid inclusion analysis in calcite crystals at Basiran, the ore-bearing solutions had relatively low salinity (<4.5 wt% NaCl eq.) and limited range of homogenization temperature (TH= 100-220°C) Which confirms the hydrothermal solution.

10
11
12
13
14
15
16
17

18

19
20

21

22

References

23

Aghanabati, A. (1998) Major sedimentary and structural units of Iran (map): Geosci. J., 7, 29-30.

24

Ahmad SN., Rose AW. (1980) Fluid inclusions in porphyry and skarn oreat Santa Rita, New Mexico. Economic Geology 75, 229–250.

25
26

Barghi, B., Calagari, A.A., Zarrinkoub, M.H. and Simmonds, V. (2017) Ore controlling parameters and genesis of Manganes Ore bodies in Southern Khorasan East of Iran. Thesis title in field economic geology, Natural science faculty geology department, University of Tabriz.

27
28
29

Bonatti, E. (1975) Metallogenesis at oceanic spreading centers. Annu. Rev. Earth. Pl. Sc., 3, 401-431.

30

Bonatti, E., Zerbi, M., Kay, R., and Rydell, H. (1976) Metalliferous deposits from the Apennine ophiolites: Mesozoic equivalent of modern deposits from oceanic spreading center. Geol. Soc. Am. Bull., 87, 83-94.

31
32

Choi, J.H. and Hariya, Y. (1992) Geochemistry and depositional environment of Mn oxide deposits in the Tokoro belt, northeastern Hokkaido, Japan. Econ. Geol., 87, 1265–1274.

33
34

Crerar, D.A., Namson, J., Chyi, M.S., Williams, L., and Feigenson, M.D. (1982) Manganiferous cherts of the Franciscan assemblage: I. General geology, ancient and modern analogues, and implications for hydrothermal convection at oceanic spreading centers. Econ. Geol., 77, 519-540.

35
36
37

Heshmatbehzadi, K., and Shahabpour, J. (2010) Metallogeny of Manganese and Ferromanganese Ores in Baft Ophiolitic Melange, Kerman, Iran. Aust. J. Earth. Sci., 4, 302-313.

38
39

Holtstam, D., and Mansfeld, J. (2001) Origin of a carbonate- hosted Fe-Mn-(Ba-As-Pb-Sb-W) deposit of Langban- type in central Sweden. Miner. Deposita., 36(7), 641-657.

40
41

Jach, R., Dudek, T. (2005) Origin of a Toarcian manganese carbonate/silicate deposit From the Krizna unit, Tatra Mountains Poland. Chem. Geol., 224, 136–152.

42
43

Maynard, J. (2010) The chemistry of manganese or through time: a signal of increasing diversity of earth-surface environments. Econ. Geol., 105, 535-552.

44
45

Mücke, A., Adjimah, K., Annor, A. (1999) Mineralogy, petrography, geochemistry and genesis of the Paleoproterozoic Birimian manganese-formation of Nsuta/Ghana. Miner. Deposita., 34, 297–311.

46
47

Nicholson, K. (1992a) Genetic types of manganese oxide deposits in Scotland: Indicators of paleo-Ocean-spreading rate and a Devonian geochemical mobility boundary. Econ. Geol., 87, 1301-1309.

48
49

Nicholson, K. (1992b) Contrasting mineralogical-geochemical signatures of manganese oxides: Guides to metallogenesis. Econ. Geol., 87, 1253-1264.

50
51

Polgari, M., Hein, J.R., Vigh, T., Szabó-Drubina, M., Fórizs, I., Bíró, L., Müller, A. and Tóth, A.L. (2012) Microbial processes and the origin of the Úrkút manganese deposit, Hungary. Ore. Geol. Rev., 47, 87-109.

Ramezani, J., Tucker, R., (2003) The Saghand region, Central Iran: U-Pb geochronology, petrogenesis and implications for Gondwana tectonics. Am. J. Sci., 303, 622-665.

Roy, S. (1992) Environments and processes of manganese deposition. Econ. Geol., 87, 1218-1236.

Roedder E. (1984) The Fluids in salt. Mineral Soc America 69, 413-439.

Roedder E. (1979)   Origion and significance of magmatic inclusions. Bull.Mineral 102, 487-510.

Stocklin, J., Nabavi, M.H., 1973. Tectonic map of Iran. Geological survey of Iran.

Spooner,E.T.C. (1981) Fluid inclusion studies of hydrothermal ore deposits. In L.S.Hollister and M.L. Crawford (eds.) Short Course in fluid Inclusions. Mineralogical Association of Canada 6, 209-510.

Tirrul, R., Bell, l. R., Griffis, J. R. & Camp, V. E., (1983) The sistan suture zone of Eastern Iran. Geological Society of America Bulletin 94, 134-150.

Toth, J. R. (1980) Deposition of submarine crusts rich in manganese and iron. Geol. Soc. Am. Bull., 91, 44-54.

Usui, A., Someya, M. (1997) Distribution and composition of marine hydrogenetic and hydrothermal manganese deposits in the northwest Pacific. In: Nicholson, K., Hein, J, R.,

Wilkinson JJ. (2001)   Fluid inclusions in hydrothermal ore deposits 55, 229–272.

Zhang YG., Frantz JD. (1987)   Determination of the homogenization temperatures and densities of supercritical fluids in the system NaCl–KCl–CaCl$_2$–H$_2$O using syntheticfluid inclusions. Chemical Geology 64, 335–350.

Zarrinkoub, M.H., Pang, K.N., Chung, S.L., Khatib, M.M., Mohammadi. S.S., Chiu, H.Y., Lee, H.Y. (2012) Zircon U/Pb age and geochemical constraints on the origin of the Birjand ophiolite, Sistan suture zone, eastern Iran. Lithos., 154, 392-405.